Understanding Precipitate Growth Kinetics at Ultra-High Hydrostatic Pressures

Siyua Cao, Naveen Weerasekera, Dawa Ram Shingdan, and Ahmed Ijaz Abdulla

***Abstract* — In this work, we have studied the precipitate growth behavior of a metal matrix when subjected to hydrostatic pressure. We utilized Zenner-Frank phase field kinetics with integrated free energy density functional based on volumetric strain energy. We studied the precipitate growth up to 2 GPa under varying bulk modulus of the precipitate phase. We observed that subjecting to hydrostatic pressure influences the growth kinetics by reducing the precipitate growth under time evolution. In addition, the bulk modulus of the precipitate has shown an abnormality in the growth behavior compared to general observations under hydrostatic pressure. This work contributes to the smart tailoring of novel materials to reduce detrimental impacts on holistic material properties, used in large hydrostatic pressure applications.**

***Keywords* — Free Energy Density Functionals, Phase Field Modeling, Precipitate Growth, Microstructure Evolution, Zenner-Frank Kinetics.**

I. INTRODUCTION

Phase field modeling (PFM) can be considered an important simulation tool for scientists and engineers to identify the evolution of microstructures under unique environments [1]. PFM stems from the classical solid state diffusion definition (Fick's law) by integrating Fick's definition to incorporate interface tracking between multiple phases. Where, PFM defines chemical potential as the driving parameter rather than the composition in classical definition [1], [2]. By incorporating chemical potential, non-classical diffusion phenomena is successfully addressed to describe experimental observations (uphill diffusion, grain growth, etc.) [1], [3].

PFM utilizes free energy of the considering system unique to a specific environment. However, general Gibbs free energy is defined only based on composition, and composition is a conserved property for any given system, therefore, non-conserved properties such as phase/microstructure are not accounted [2], [4]. To address the contributions from both composition and microstructure, in PFM, free energy is defined as a free energy functional (FF). In this approach, total free energy is embedded as a function of chemical-free energy and interfacial diffusion processes of composition and microstructures [2]. Due to this definition, FF helped tremendously in defining unique properties specific to a phase system not only based on internal or chemical contributions but under external fields (uniaxial stress, hydrostatic pressure, electric field, etc.) [2], [3], [5]–[7].

We extract a few previous works performed based on defining free energy density unique to specific external conditions. Initially, PFM to study precipitate growth at uniaxial stresses is soundly demonstrated by Mukherjee *et al*. [2]. They utilized Zenner-Frank (ZF) phase field kinetics under elastic strain energy contributions to FF. Secondly, precipitate kinetics under thermal energy such as isothermal aging is widely studied by Weerasekera *et al*. [1], [3]. They have also used ZF kinetics to address the phenomena. Ohno *et al*. [8] studied phase transformations in the steel welding process using Kurz-Giovanola-Trivedi (KGT) model. They used the KGT integrated FDF to define the solid-fluid multiphase transformation process. Yang *et al*. [5] studied phase transformation kinetics of the electron power bed fusion process [9]. They defined the FDF using a powder scale thermal fluid flow model (TFF) to address the problem. Based on all such contributions, PFM as a study tool for phase transformation problems is widely used by the modern research community [4], [6], [10]–[15].

Through this study, we are closing another research gap on precipitate growth kinetics which are at extreme hydrostatic pressures (> 0.1 GPa). Microstructure evolution at hydrostatic pressures is highly important for many engineering and commercial applications [11], [16] to observe material property

Submitted on April 15, 2022.
Published on May 17, 2022.
S. Cao, Department of Mathematics and Statistics, Portland State University, USA.
N. Weerasekera, Department of Mechanical Engineering, University of Louisville, USA.
D. R. Shingdan, Department of Environmental Sciences, Nagoya University, Japan.
A. I. Abdulla, Department of Mechanical Engineering, National Institute of Technology-Silchar, India.
(corresponding e-mail: naveen12.weerasekera@louisville.edu)

behavior in such environments. By identifying this necessity, we have developed a PFM using ZF phase-field kinetics with novel modifications to FF to account the influence of hydrostatic pressure on precipitate growth. To develop the FF we sheltered from the approach by Mukherjee *et al*. [2] which is based on defining FF accounting for uniaxial strain energy. Fig. 1 shows a schematic of a typical scenario where hydrostatic pressure is applied to a solid material.

In this work, we have demonstrated the impact of hydrostatic pressure using an evolution of a precipitate grown in a bulk matrix phase. We studied multiple scenarios by varying hydrostatic pressures as well as the different bulk modulus for each phase to study precipitate evolution behavior.

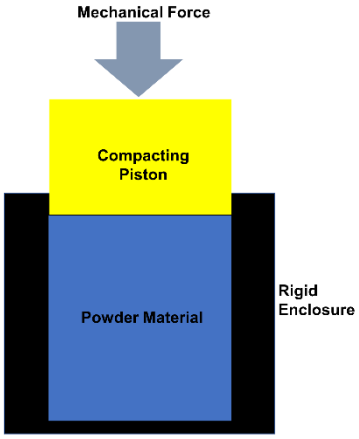

Fig. 1. A solid material subjected to hydrostatic pressure under confinement. (Application: Powder compaction process in powder metallurgy).

II. Phase Field Model only with Chemical Contribution

As introduced in the previous section, we are utilizing the ZF PFM model with a double-well type free energy density function for composition (c) in the form of $f = Ac^2(1-c)^2$ [2]. Each minimum of this function represents the stable composition of each phase. However, the above free energy density function accounts only for the composition, where the contributions to free energy from the microstructure or an individual phase are neglected. To include the phase properties, ZF PFM defines free energy density as a function of both composition and microstructure order parameter (η) using an additional speciality function referred as Wang function [1].

For the ZF PFM, the composition is evolved using the Cahn-Hilliard (CH) equation as [1]:

$$\frac{\partial c}{\partial t} = M\nabla^2\left(\frac{\partial (F/N)}{\partial c}\right) \tag{1}$$

where, F/N is the free energy functional normalized per atom (Where N is the number of atoms per unit volume in the system- which is referred to as the free energy density functional (FDF)) which only accounts for the chemical contribution [2]. Secondly, the microstructure order parameter (η) is evolved using Alan-Cahn equation as [1]:

$$\frac{\partial \eta}{\partial t} = -L\left(\frac{\partial (F/N)}{\partial \eta}\right) \tag{2}$$

where, L is the interface mobility considered for the microstructure (phase) order parameter. Free energy density functional (F/N) for ZF model can be given as:

$$\frac{F}{N} = \int \{f(c,\eta) + k_c(\nabla c)^2 + k_\eta(\nabla \eta)^2\}.dV \tag{3}$$

where, $f(c,\eta)$ is the bulk free energy of the system and k_c is the gradient energy coefficient for composition which is different from the diffusion coefficient applied in Fick's law. k_η is the gradient energy coefficient of the microstructure order parameter which is unique for the system. The bulk free energy density function can be written using the dual minimum approach using Wang function $W(\eta)$ as [1], [2]:

$$f(c,\eta) = f^m(c)(1-W(\eta)) + f^p(c)W(\eta) + P\eta^2(1-\eta)^2 \tag{4}$$

With P as a constant, $f^m(c)$ represents the free energy of the bulk phase (matrix) and $f^p(c)$ represents the free energy of the precipitate phase. $f^m(c)$ and $f^p(c)$ are modeled simply using quadratic functions to implement the effect of double-well potential and subsequent spinodal decomposition as $f^m(c) = Ac^2$ and $f^p(c) = B(1-c)^2$ [2]. To implement F/N in Cahn-Hilliard and Alan-Cahn equations, derivatives with respect to c and η of F/N can be given as:

$$\frac{\partial(F/N)}{\partial c} = \frac{\partial f(c,\eta)}{\partial c} - 2k_c\nabla^2 c \tag{5}$$

$$\frac{\partial(F/N)}{\partial \eta} = \frac{\partial f(c,\eta)}{\partial \eta} - 2k_\eta\nabla^2 \eta \tag{6}$$

In similar fashion, derivatives of free energy density function with respect to c and η can be given as:

$$h_c = \frac{\partial f(c,\eta)}{\partial c} = 2Ac(1-W(\eta)) - 2B(1-c)W(\eta) \tag{7}$$

$$h_c = \frac{\partial f(c,\eta)}{\partial c} = 2Ac(1-W(\eta)) - 2B(1-c)W(\eta) \tag{8}$$

$$h_\eta = \frac{\partial f(c,\eta)}{\partial \eta} = 2Ac^2W(\eta) - B(1-c)^2W'(\eta) + 2P\eta(1-\eta)(1-2\eta) \tag{9}$$

where, Wang function, $W(\eta)$ and its derivative $W'(\eta)$ can be obtained according to:

$$W(\eta) = \begin{cases} 0 & \text{If } \eta < 0 \\ \eta^3(10-15\eta+6\eta^2) & \text{If } 0 \le \eta \le 1 \\ 1 & \text{If } \eta > 1 \end{cases}$$

$$W'(\eta) = \begin{cases} 0 & \text{If } \eta < 0 \\ 3\eta^2(10-15\eta-16\eta^2)+\eta^3(12\eta-15) & \text{If } 0 \le \eta \le 1 \\ 0 & \text{If } \eta > 1 \end{cases}$$

III. Phase Field Model with Hydrostatic Contribution

In the previous section, we have only considered the chemical contribution to FDF without any influence from external factors as introduced before. We can modify the ZF FDF to include influence from hydrostatic pressure similar to the approach introduced by Mukherjee *et al*. [2] based on uniaxial stress. It is important to note that in a uniaxial case, we are mainly concerned about the uniaxial strain to define strain energy, while at hydrostatic pressure, strain energy is defined based on volumetric strain. Therefore, for a hydrostatic pressure case, strain energy can be defined as:

$$F^{vd} = \frac{1}{2}\int_V p.\frac{\Delta v}{v_0}\,dV \tag{10}$$

where, p is the hydrostatic pressure, which is isotropic unlike uniaxial stress in the domain; $\frac{\Delta v}{V_0}$ is a hydrostatic strain which is written as γ from hereafter; V_0 is the initial volume before deformation. By knowing the bulk modulus of the system (B), we can write the relation between p and γ as:

$$p = B.\gamma(\eta) \tag{11}$$

The dependence of microstructure order parameter (η) on hydrostatic strain can be correlated using a scaler interpolation function ($\beta(\eta)$) unique to the system, similar to Mukherjee *et al*. [2]:

$$\gamma(\eta) = \beta(\eta).\gamma \tag{12}$$

We model the ($\beta(\eta)$) function associated with ZF kinetics similar to Mukherjee *et al*. [2] as:

$$\beta(\eta) = \eta^3(10-15\eta+6\eta^2) - \frac{1}{2} \tag{13}$$

Secondly, not only the hydrostatic strain, but dependence of bulk modulus with order parameter can also be attributed using a second interpolation function ($\delta(\eta)$) as:

$$B = B^{eff} + \delta(\eta).(B^{p} - B^{m}) \tag{14}$$

where, B^{p} and B^{m} are bulk modulus of p and m phases respectively. Also, B^{eff} is the effective bulk modulus and can be modeled as $B^{eff} = (B^{p} + B^{m})/2$ [2].Therefore, based on these relations, we developed the final relation for F^{vd} as:

$$F^{vd} = \frac{1}{2}\int_{V} B^{eff} + \delta(\eta).(B^{p} - B^{m}).\beta(\eta)^{2}.\gamma^{2} \tag{15}$$

Therefore, we present the total FDF by adding the above results below as:

$$\frac{F}{N} = \int \left\{ f(c,\eta) + k_c(\nabla c)^2 + k_\eta(\nabla\eta)^2 + \frac{1}{2}[B^{eff} + \delta(\eta).(B^{p} - B^{m}).\beta(\eta)^{2}.\gamma^{2}] \right\}.dV \tag{16}$$

Here we again note that the free energy density function $f(c,\eta)$ will be considered the same as before (4) since the free energy density function is defined only using the thermodynamic behavior of the atomic structure [1]. Therefore, the derivative of FDF with respect to c ($\frac{\partial(F/N)}{\partial c}$), is similar to (5). However, derivative of FDF with respect to η takes the form as below while considering $\delta(\eta)$ as a constant [2]:

$$\frac{\partial(F/N)}{\partial\eta} = \frac{\partial f(c,\eta)}{\partial\eta} - 2k_\eta\nabla^2\eta + 2.\delta(\eta).(B^{p} - B^{m}).\beta(\eta).\frac{d\beta(\eta)}{d\eta}\,\gamma^{2} \tag{16}$$

We can now rewrite the new Alan-Cahn equation with the above modifications as:

$$\frac{\partial\eta}{\partial t} = -L\{\frac{\partial f(c,\eta)}{\partial\eta} - 2k_\eta\nabla^2\eta + 2.\delta(\eta).(B^{p} - B^{m}).\beta(\eta).\frac{d\beta(\eta)}{d\eta}\,\gamma^{2}\} \tag{17}$$

IV. Solution Process and Computational Code Development

We have developed a code using MATLAB software incorporating Fourier spectral techniques with periodic boundary conditions in 2D space. We solved Cahn-Hilliard (1) and modified Alan-Cahn (17) equations under different hydrostatic pressure conditions and phase properties (Bulk modulus). We created a simulation domain with 64 grid points in the x-y space with a hypothetical square specimen sample of 0.5 mm inside length.

The Fourier spectral technique transforms the process variables which are in time-space to the frequency space [17]. By performing such transformation, the complexity of Cahn-Hilliard and Alan-Cahn equations can be reduced to first-order differential equations, where seeking a solution becomes more convenient compared to its original form. The Fourier spectral technique for Cahn-Hilliard equation can be given as:

$$\frac{\partial\tilde{c}}{\partial t} = -Mk^{2}\tilde{c} \tag{18}$$

where, $\tilde{c}$ is the composition in Fourier space after the Fourier transform is performed. Computationally it is performed using the Fast Fourier Transform (FFT) techniques [17]. And k is the wave vector. Now, we can discretize Equation 18 in the time domain to be evolved in time space with a time step of dt as"

$$\tilde{c}^{t+dt} = \frac{\tilde{c}^{t}}{1 + Mk^{2}dt} \tag{19}$$

Secondly, we can follow a similar process to transform Alan-Cahn equation to frequency space as:

$$\frac{\partial\tilde{\eta}}{\partial t} = -2k_\eta Lk^{2}\tilde{\eta} - L\tilde{g} \tag{20}$$

where, $\tilde{\eta}$ is the microstructure order parameter in the Fourier space and $\tilde{g}$ is the Fourier transformed function of $\frac{\partial f(c,\eta)}{\partial \eta}$. We can again discretize the Equation 20 to be evolved in the time space as:

$$\tilde{\eta}^{t+dt} = \frac{\tilde{\eta}^{t} - Ldt\tilde{g}}{1 + 2k_{\eta}Lk^{2}} \tag{21}$$

For all simulations, we choose iron as the base material. And we applied a general value of bulk modulus of iron – 266.1 GPa [18] to obtain volumetric strains for different applied hydrostatic pressures using Equation 11 and also, and this value is considered as the bulk modulus of the matrix phase (*m*-phase). For two different phases, we attributed a bulk modulus which is deviating from the pure bulk modulus of 266.1 GPa as presented in Table I. In addition, we applied a constant value of 0.5 for the second interpolation function $\delta(\eta)$, to reduce the complexity of the analysis [2].

TABLE I: CASE STUDIES FOR DIFFERENT SIMULATIONS

Hydrostaic Pressure	Bulk Modulus of *p* phase, (B^p)			Bulk Modulus of *m* phase, (B^m)
	Case Study -1	Case Study -2	Case Study -3	
0.1 GPa	50 GPa	100 GPa	150 GPa	266.1 GPa
1 GPa	50 GPa	100 GPa	150 GPa	266.1 GPa
2 GPa	50 GPa	100 GPa	150 GPa	266.1 GPa

We have initially developed a circular precipitate centered in the simulation domain with a radius of 0.1 mm as shown in Fig. 2. We attributed *p*-phase properties to the precipitate while the matrix phase is attributed with *m*-phase properties. The simulations are performed for each case study with a non-dimensional time step of 0.5 with 125 time steps similar to our previous work on ZF phase field kinetics of precipitate growth [1]. For all simulations, we assumed a value of unity for the coefficients *M*, *L*, k_c and k_η, since these values do not interfere with the qualitative understanding of the problem. We have studied the growth behavior of the precipitate under case studies as presented in Table I.

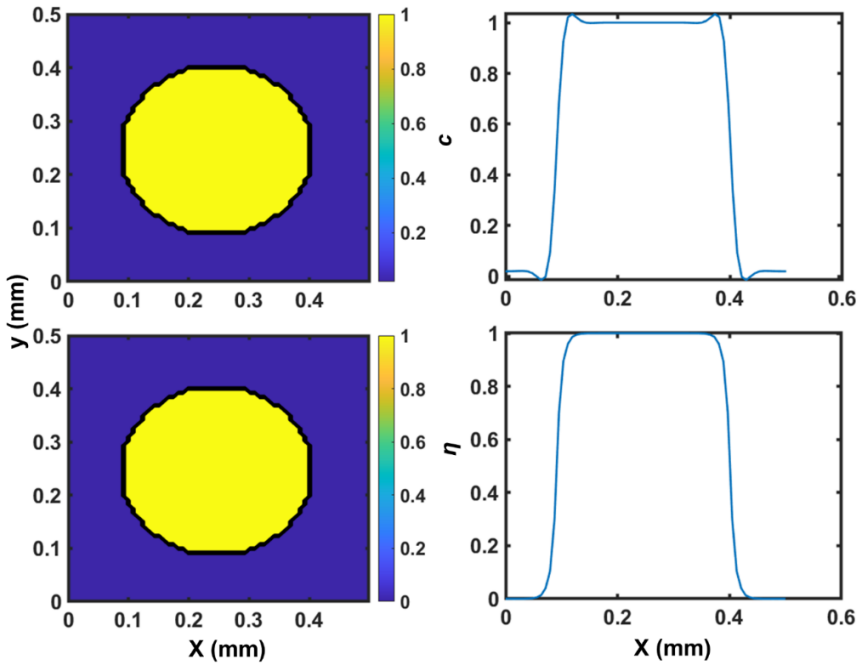

Fig. 2. Initial profiles of the circular precipitates attributed with *p*-phase properties for all simulations.

V. RESULTS AND DISCUSSION

Fig. 3 presents the composition and microstructure order parameters of the precipitate growth at zero pressure conditions. As in our previous work [1], for this scenario, ZF model only accounts the chemical contributions. Therefore, we observe the simple precipitate growth behavior influenced by an uphill diffusion process. We used this free growth process as the baseline case to compare the impact of pressure on the growth of the precipitate. Fig. 4–6 shows time evolved contours of microstructure order parameters for different scenarios as presented in Table I. It is important to note that even with hydrostatic pressure, time-evolved composition contours stay similar to the base case due to the vanishing of external terms while taking derivatives (Equation 1) validating its conserved nature.

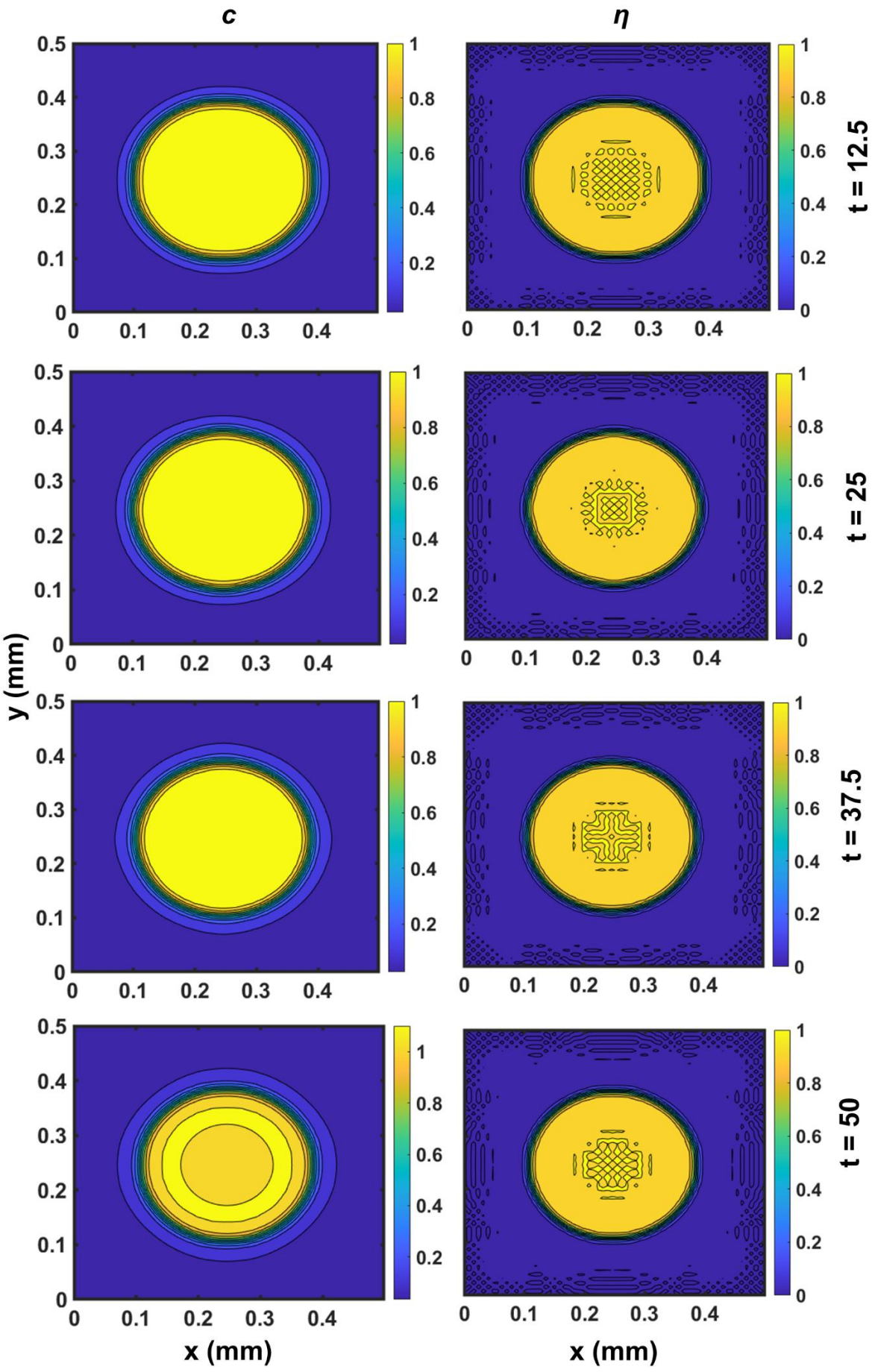

Fig. 3. Growth of the precipitate without external contributions – composition and microstructure order parameter varied with non-dimensionalized time *t*.

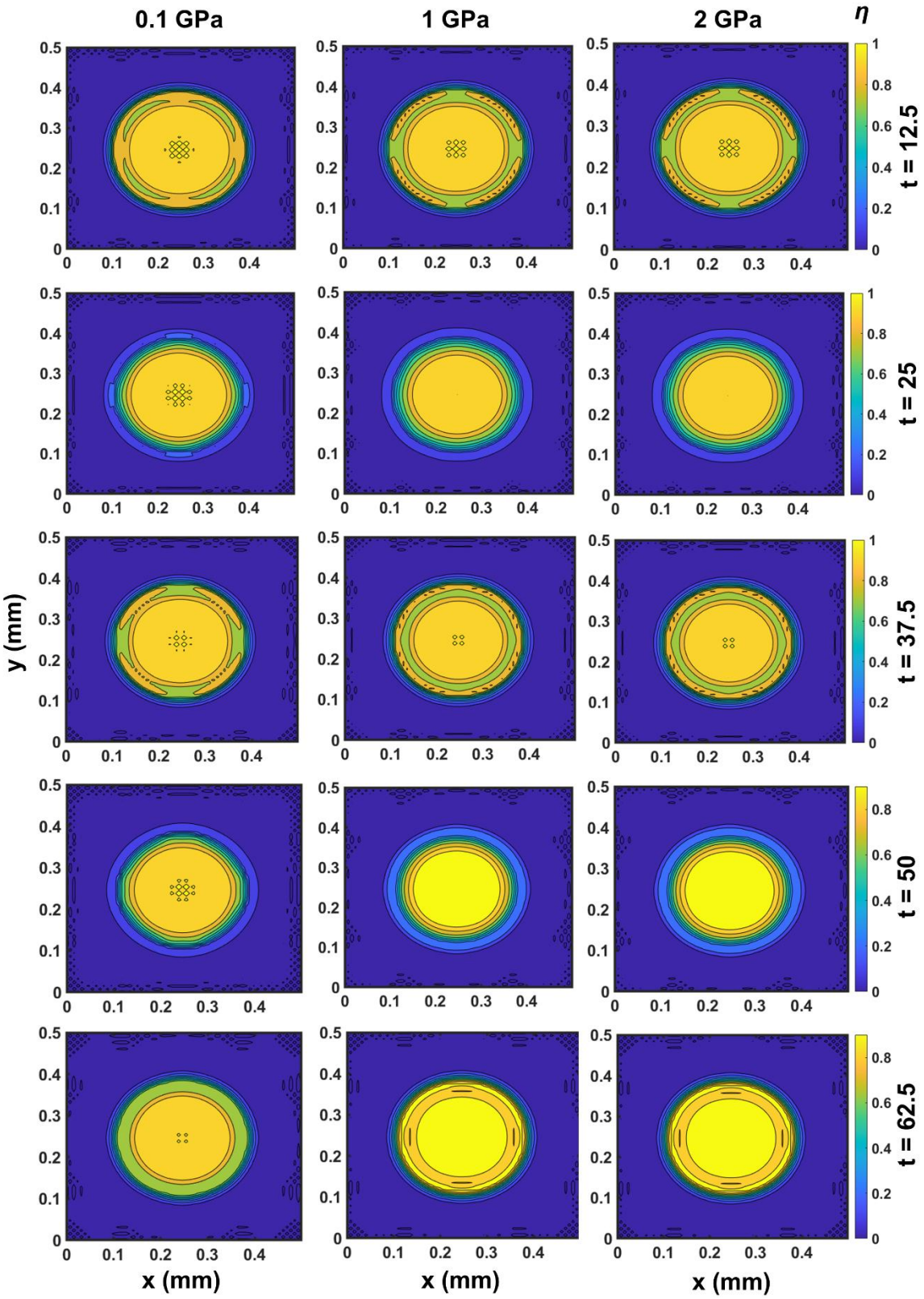

Fig. 4. Growth of the precipitate under hydrostatic pressure. Evolution of the microstructure order parameter for multiple pressures (0.1 to 2 GPa) with B = 50 GPa as in case study 1.

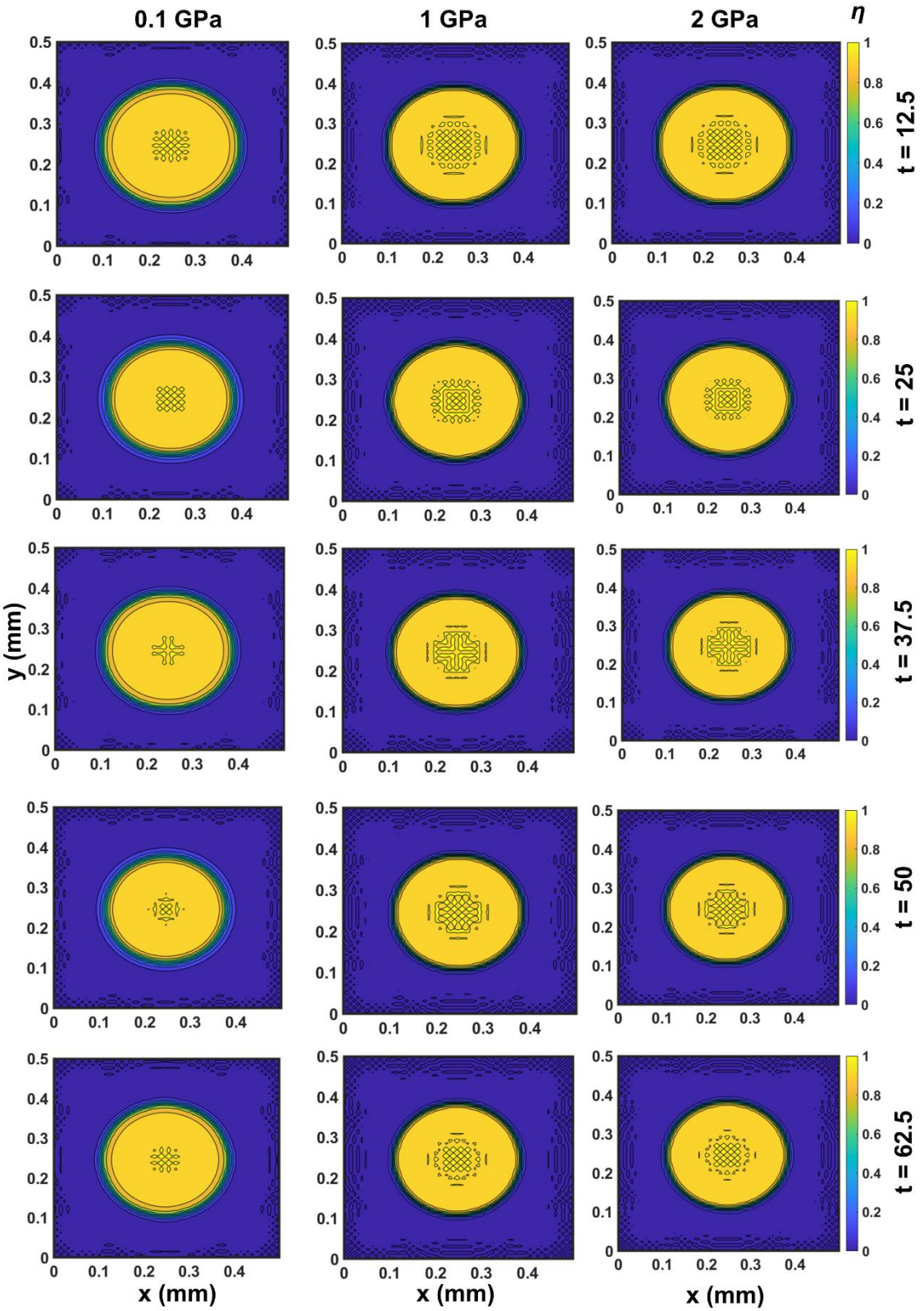

Fig. 5. Growth of the precipitate under hydrostatic pressure. Evolution of the microstructure order parameter for multiple pressures (0.1 to 2 GPa) with B = 100 GPa as in case study 2.

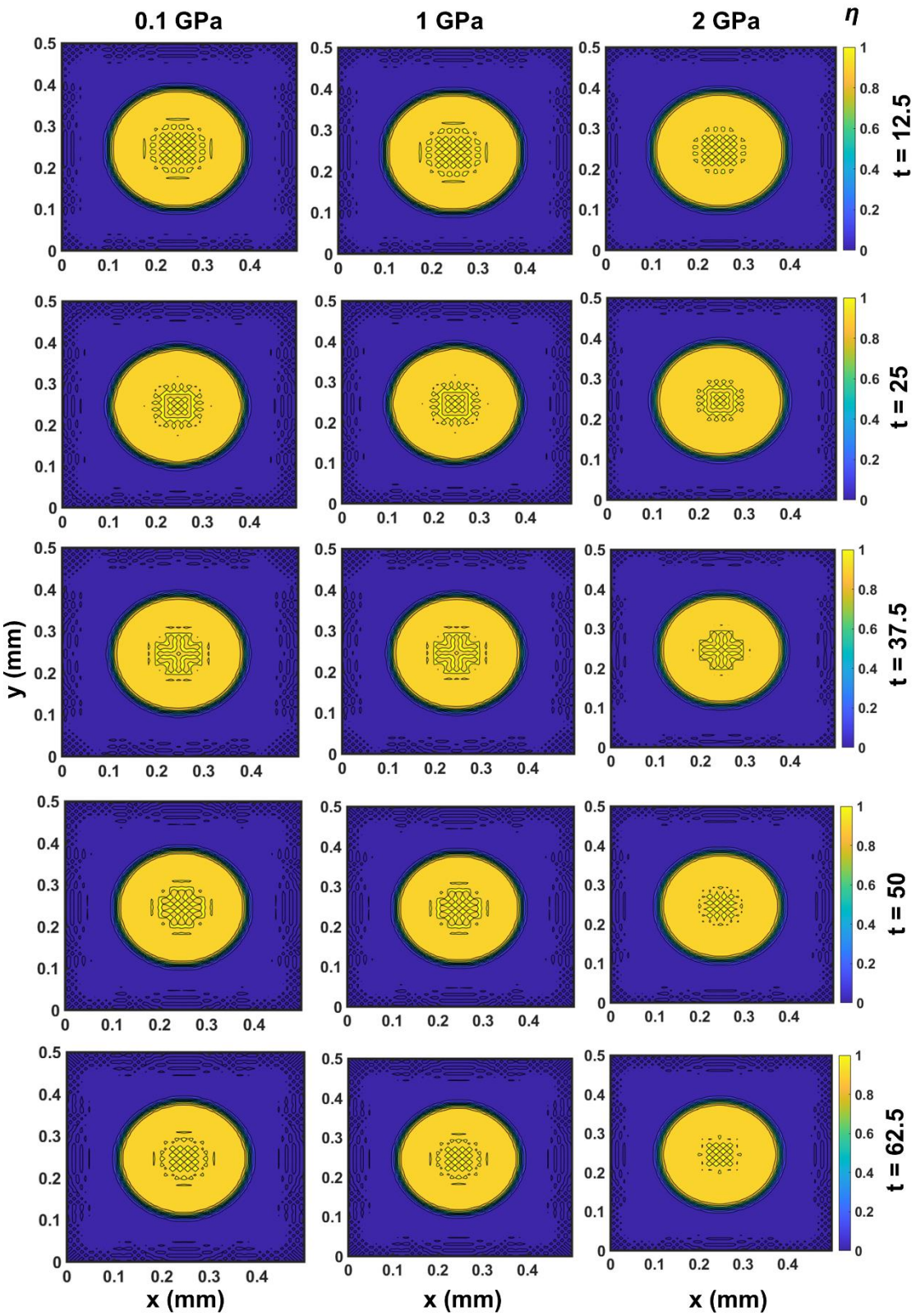

Fig. 6. Growth of the precipitate under hydrostatic pressure. Evolution of the microstructure order parameter for multiple pressures (0.1 to 2 GPa) with B = 150 GPa as in case study 3.

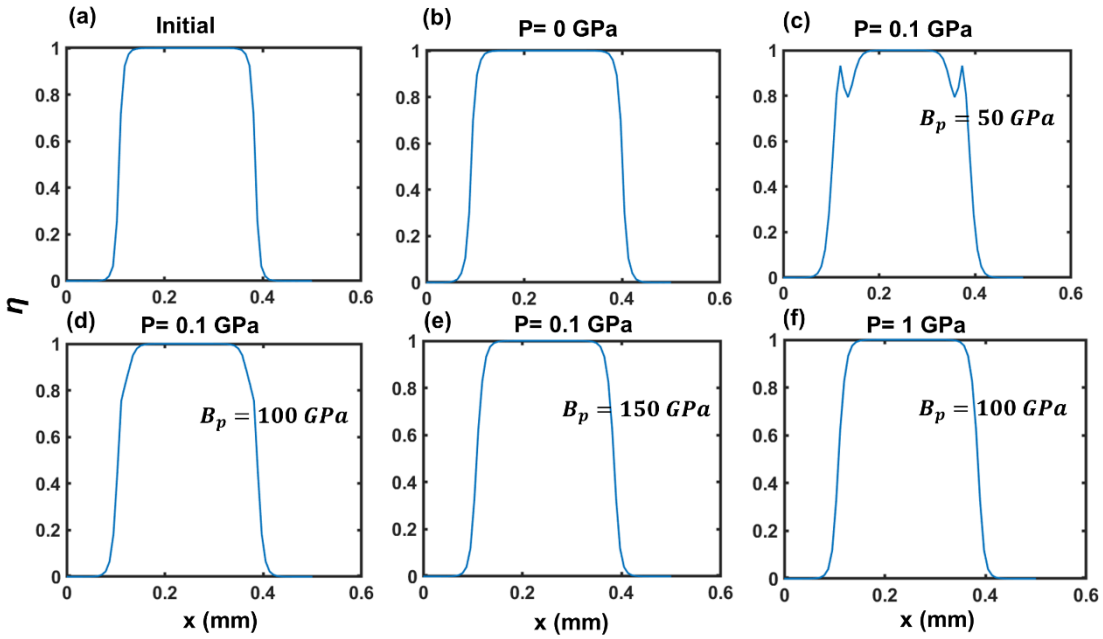

Fig. 8. Analysis of the growth front with and without hydrostatic pressure for multiple pressure and phase properties (Bulk modulus).

Initially, when observing the growth of the precipitate holistically, we identify that maximum growth is possible only at zero pressure conditions. The application of pressure has significantly reduced the growth compared to free conditions. Specifically, when comparing the evolution of the precipitate as shown in Fig. 8, a-b-d and f, for the same bulk modulus of 100 GPa, with the increasing pressure up to 1 GPa, we observe that the growth front stayed stationary compared to the free case. In addition, the shape of the precipitate has changed from the initial profile to a more peaked shape (Fig. 8, a-b-d-f). Secondly, the application of pressure for the same bulk modulus impacted the growth by reducing nucleation inside the precipitate as observed in Fig. 4–6, 0.1–2 GPa with increasing pressure under all case studies. As in Fig. 8, a-b-c-d and e, change of the bulk modulus from 50 to 150 GPa mainly impacted the shape of the precipitate. For B_p of 50 GPa (Fig. 8-c), an abnormal shape defect is observed inside the precipitate. However, as we increase the B_p value from 50 GPa to 266.1 GPa, the change in the precipitate profiles reaches almost to the initial profile (Fig. 8-a).

These observations are more clearly identifiable while studying the contour plots of the evolution (Fig. 4–6). When focusing on all case studies evolved at a pressure of 2 GPa, the nucleation rate at the middle of the precipitate has reduced tremendously. The more abnormality of the shape is observed when a great difference between the bulk modulus of precipitate and matrix phase is applied (50–266.1 GPa).

We can successfully identify the kinetics of current growth behavior by focusing on the FDF. Initially, a transition from *m*-phase to *p*-phase needs activation to observe the growth of the precipitate. The *m*-phase demonstrates lower free energy and therefore, additional energy is required to overcome the free energy gap while transitioning from *m*-phase to *p*-phase. Integrating hydrostatic pressure provides additional energy to the system as demonstrated in FDF (16). However, such additional energy is not provided as an excitation, but as a contraction, contrary to thermal energy as studied in our previous works [1]. Applying large hydrostatic pressures reduces the amplitude of the molecular vibrations and subsequently reduces the kinetic contributions to the free energy of the system, where the free energy of the dispersed phase (*m*-phase) becomes dominant while averaging volumetrically. By this effect, transitioning from *m*-phase to *p*-phase becomes more challenging as we observe in this study.

As the crucial importance of this study, for a metallurgist who is developing new materials for research and engineering applications, those materials subjecting to large hydrostatic pressures, can demonstrate change in microstructure oriented functional properties [13] as we studied through this work. Internal defects with large bulk modulus differences can cause abnormalities in overall mechanical properties and may even cause failure. Therefore, smart tailoring of the new material is required for failure-proof designs under such circumstances. Environmental impacts such as corrosion can also cause the formation of abnormal precipitates that can result in abnormal growth behaviors.

VI. Conclusion

In this work, we have studied precipitate growth kinetics under hydrostatic pressures. We have produced a circular precipitate in a bulk matrix phase and observed its evolution with multiple scenarios. We implemented hydrostatic pressure conditions by integrating volumetric strain energy to the free energy density functional defined by Zenner-Frank phase field kinetics. We initially evolved the precipitate without any applied pressure, in the non-dimensionalized time space to be considered as the base case. Subsequently, we studied the evolution of the same precipitate subjected to a hydrostatic pressure up to 2 GPa. Furthermore, we have varied the bulk modulus of the precipitate to observe any impact on the precipitate growth. We found that hydrostatic pressure reduces the development of the growth front compared to the base case. In addition, deviating the bulk modulus of the precipitate further away from the matrix phase produces abnormalities in growth behavior as well as in homogeneity. Based on these results, we conclude that precipitates with large property variations can impact holistic material properties such as tensile strength, thermal expansion, etc. under the application of large hydrostatic pressures. Therefore, it at utmost importance to track material microstructure changes while at extreme environmental applications.

Acknowledgment

Authors wish to thank Dr. Laksman Perera at the Department of Physics and Astronomy of the University of Colombo, Sri Lanka, for reviewing this work and providing valuable feedback.

Conflict of Interest

Authors declare that they do not have any conflict of interest.

AUTHOR CONTRIBUTIONS

S. Cao and N. Weerasekera conceptualized the project and performed phase field simulations. D. Shingdan and A. Abdulla assisted with simulations. S. Cao and N. Weerasekera wrote the paper from the input of all authors.

References

[1] Weerasekera N., Cao S., and Shingdon D. R. Phase Field Modeling of Ghost Diffusion in Sn-Ag-Cu Solder Joints. *European Journal of Applied Physics*, 2022; 4(2):28–34. doi: http://dx.doi.org/10.24018/ejphysics.2022.4.2.163.
[2] Mukherjee R., Abinandanan T. A., and Gururajan M. P. Phase field study of precipitate growth: Effect of misfit strain and interface curvature. *Acta Materialia*, Aug. 2009;57(13):3947–3954. doi: 10.1016/j.actamat.2009.04.056.
[3] Weerasekera N. and Abdulla A. Application of Zenner-Frank Phase Field Theory for Simulating Cu Depletion Effect in Isothermally Aged SAC BGA Solder Joints. *International Journal of Scientific and Engineering Research*, 2019;10(11):1210–1216.
[4] Gomez H., Bures M., and Moure A. A review on computational modelling of phase-transition problems. *Phil. Trans. R. Soc. A.*, Apr. 2019;377(2143):20180203. doi: 10.1098/rsta.2018.0203.
[5] Yang M., Wang L., and Yan W. Phase-field modeling of grain evolutions in additive manufacturing from nucleation, growth, to coarsening. *npj Comput Mater*, Dec. 2021;7(1):56. doi: 10.1038/s41524-021-00524-6.
[6] Jafari R. and Okutucu-Özyurt T. Phase-Field Modeling of Vapor Bubble Growth in a Microchannel. *The Journal of Computational Multiphase Flows*, Sep. 2015;7(3):143–158. doi: 10.1260/1757-482X.7.3.143.
[7] Wang Q., Zhang G., Li Y., Hong Z., Wang D., and Shi S. Application of phase-field method in rechargeable batteries. *npj Comput Mater*, Dec. 2020;6(1):176. doi: 10.1038/s41524-020-00445-w.
[8] Ohno M., Shibuta Y., and Takaki T. Multi-Phase-Field Modeling of Transformation Kinetics at Multiple Scales and Its Application to Welding of Steel. *Mater. Trans.*, Feb. 2019;60(2):170–179. doi: 10.2320/matertrans.ME201711.
[9] Weerasekera N., Cao S., and Biswas A. Issues in Resolution and Build Size Scaling of Additive Manufacturing Technologies. *Open Science Journal*, 2022;7(1):31. doi: 10.23954/osj.v7i1.3092.
[10] Feng L., Zhong J., Zhu C., Wang J., An G., and Xiao R. Multi-phase field simulation of multi-grain peritectic transition in multiple phase transformation. *China Foundry*, Sep. 2020;17(5):357–363. doi: 10.1007/s41230-020-9136-0.
[11] Weerasekera N. Particle Level Material Characterization of Neopentyl Glycol (NPG) For Intermediate Thermal Energy Storage. Presented at the Kentucky Regional Research Conference, Louisville, Kentucky, USA, Mar. 2021. doi: 10.13140/RG.2.2.32529.71520.
[12] Chen L.-Q. Phase-Field Models for Microstructure Evolution. *Annu. Rev. Mater. Res.*, Aug. 2002;32(1):113–140. doi: 10.1146/annurev.matsci.32.112001.132041.
[13] Weerasekera N., Cao S., and Perera L. Functional Property Evaluation of Crystalline Materials using Density Functional Theory: A Review. *EJPHYSICS*, Jan. 2022;4(1):19–26. doi: 10.24018/ejphysics.2022.4.1.142.
[14] Weerasekera N. D.and Laguerre A. Coupled Continuum Advection-Diffusion Model for Simulating Parallel Flow Induced Mass Transport in Porous Membranes. *IJSR*, 2019;8(12):694–700. doi: 10.21275/ART20203395.
[15] Weerasekera N. D. and Cao S. Multifaceted Convergence Study for Evaluating Gas Diffusion Parameters of Polymeric Membranes. *IJEAS*, Nov. 2019;6(11). doi: 10.31873/IJEAS.6.11.21.
[16] Aznar A. *et al.* Reversible and irreversible colossal barocaloric effects in plastic crystals. *J. Mater. Chem. A*, 2020;8(2). doi: 10.1039/C9TA10947A.

[17] Baskakov A. G., Krishtal I. A., and Romanova E. Yu. Spectral analysis of a differential operator with an involution. *J. Evol. Equ.*, Jun. 2017;17(2):669–684. doi: 10.1007/s00028-016-0332-8.
[18] A. Rajabpour, L. Seidabadi, and M. Soltanpour. Calculating the Bulk Modulus of Iron and Steel Using Equilibrium Molecular Dynamics Simulation. *Procedia Materials Science*, 2015;11:391–396. doi: 10.1016/j.mspro.2015.11.005.

Siyua Cao is a doctoral candidate at the Department of Mathematics and Statistics of Portland State University, Portland, OR. He has completed his master's degree in mathematics from Portland State University. He currently works as a research and teaching assistant at Portland State University. His research interests fall on advanced approaches to obtain solutions to many-body Schrǿdinger equation by numerical approaches. He utilizes statistical as well as numerical approaches to conduct his research.

Naveen Weerasekera is a doctoral candidate at the Department of Mechanical Engineering of University of Louisville, Louisville, KY, USA. He has completed his Master's degree in mechanical engineering from Portland State Univerisity, Portland, OR. He is currently working as a departmental research assistant at University of Louisville under multiple fellowships. His research interests fall to solid state refrigeration devices, advanced phase change processes and evaluating material properties of functional materials for efficient caloric cooling. He utilizes experimental, analytical as well as numerical approaches to asses functional properties of materials

Dawa Ram Shingdan is a doctoral candidate at the Department of Environmental Sciences of Nagoya University, Nagoya, Japan. He completed his undergraduate degree in Mechanical Engineering from National Institute of Technology-Silchar, Assam, INDIA. He currently works as a research and teaching assistant at the Nagoya University. His research interests are based on solar thermal renewable energy systems and microscopic modeling of heat transfer.

Ahmed Ijaz Abdulla obtained his Bachelor's and Master's degree in Mechanical Engineering from National Institute of Technology – Silchar, Assam, INDIA. He worked as a former graduate research assistant at the Department of Mechanical Engineering of NIT-Silchar. He performed his graduate research on molecular dynamics and phase field modeling by colloborating with Dr. S. Halder Department of Mechanical Engineering of NIT-Silchar.